

Critical slowing down in purely elastic ‘snap-through’ instabilities

Michael Gomez, Derek E. Moulton and Dominic Vella*

Mathematical Institute, University of Oxford, Woodstock Rd, Oxford, OX2 6GG, UK

Many elastic structures have two possible equilibrium states [1]: from umbrellas that become inverted in a sudden gust of wind, to nano-electromechanical switches [2, 3], origami patterns [4, 5] and the hopper popper, which jumps after being turned inside-out [6]. These systems typically transition from one state to the other via a rapid ‘snap-through’. Snap-through allows plants to gradually store elastic energy, before releasing it suddenly to generate rapid motions [7, 8], as in the Venus flytrap [9]. Similarly, the beak of the hummingbird snaps through to catch insects mid-flight [10], while technological applications are increasingly exploiting snap-through instabilities [11–13]. In all of these scenarios, it is the ability to repeatedly generate fast motions that gives snap-through its utility. However, estimates of the speed of snap-through suggest that it should occur more quickly than is usually observed. Here, we study the dynamics of snap-through in detail, showing that, even without dissipation, the dynamics slow down close to the snap-through transition. This is reminiscent of the slowing down observed in critical phenomena, and provides a handheld demonstration of such phenomena, as well as a new tool for tuning dynamic responses in applications of elastic bistability.

Snap-through occurs when a system is in an equilibrium state that either ceases to exist or becomes unstable as a control parameter varies: the system must jump to another equilibrium state. For example, in the Venus flytrap it is believed that the natural curvature of the leaf changes slightly making the ‘open’ equilibrium disappear leaving only the ‘closed’ equilibrium [9].

Bistability and snap-through can be demonstrated using an elastic strip of length L whose edges are clamped at equal angles $\alpha \neq 0$ to the horizontal (Fig. 1a) [14, 15]. Provided that the two ends of this arch are brought together by a large enough distance ΔL , two stable shapes exist: the ‘natural’ mode and an ‘inverted’ shape (Fig. 1a). However, as ΔL is gradually decreased (pulling the two ends apart), the inverted equilibrium shape suddenly snaps through to the natural shape. The bifurcation diagram for this system (Fig. 1a) shows that as ΔL is decreased the inverted state becomes unstable, before ceasing to exist at still smaller ΔL .

Snap-through due to an equilibrium state becoming unstable, as in the above example, is generally amenable

to linear stability analysis [6, 16]: the displacement of each point on the arch evolves in time as $\sim e^{\sigma t}$ for some growth rate σ . The more dynamically interesting snap-through occurs when an equilibrium state ceases to exist without first becoming unstable (known as a saddle-node/fold bifurcation or limit-point instability [17]). This textbook snap-through [1] can be obtained simply by holding one end of the strip horizontally, while the other remains clamped at the angle α (Fig. 1b).

The change in bifurcation to a saddle-node type means that a standard linear stability analysis no longer applies. Many previous works adopt a purely numerical approach to study the dynamics in this scenario [14]. In a simple elastic model, transverse displacements $w(x, t)$ of the strip are governed by the dynamic beam equation:

$$\rho_s h \frac{\partial^2 w}{\partial t^2} + B \frac{\partial^4 w}{\partial x^4} + P \frac{\partial^2 w}{\partial x^2} = 0, \quad 0 < x < L, \quad (1)$$

with the material properties of the strip denoted by ρ_s (density), h (thickness) and $B = Eh^3/12$ (bending stiffness, with E the Young’s modulus); P is the applied compressive load (per unit width). An alternative approach is to estimate the time scale of snapping by balancing the first two terms in (1), suggesting that snap-through should occur on a time scale

$$t_* = \left(\frac{\rho_s h L^4}{B} \right)^{1/2} \sim \frac{L^2}{h \sqrt{E/\rho_s}}. \quad (2)$$

This time scale involves the speed of sound within the strip, $(E/\rho_s)^{1/2}$, and so is typically very short. However, the above estimate frequently overestimates the speed of snapping, with the discrepancy attributed to some form of dissipation [9, 14]. We investigate this snap-through ‘bottleneck’ using a controlled version of our handheld snapping experiment and detailed analysis of (1).

We performed experiments on thin strips of polyethylene terephthalate (PET) and stainless steel shim (see Methods). A strip is clamped (with ends angled appropriately) and then buckled into an arch by imposing an end-shortening ΔL (Fig. 2a). Snap-through is reached by altering ΔL quasi-statically to values $\Delta L < \Delta L_{\text{fold}}$, with the threshold ΔL_{fold} determined experimentally (see appended Supplementary Information for details). To obtain repeatable experiments with a given value of $\Delta L < \Delta L_{\text{fold}}$, the strip is initially prevented from snapping by an indenter that fixes the displacement of the midpoint to be that at the bifurcation point, $w_{\text{fold}}(L/2)$. On removing the constraint, the strip then snaps from rest (Fig. 2b).

A spatio-temporal plot of the midpoint position during snap-through (Fig. 2c) reveals the nonlinear nature of

* dominic.vella@maths.ox.ac.uk

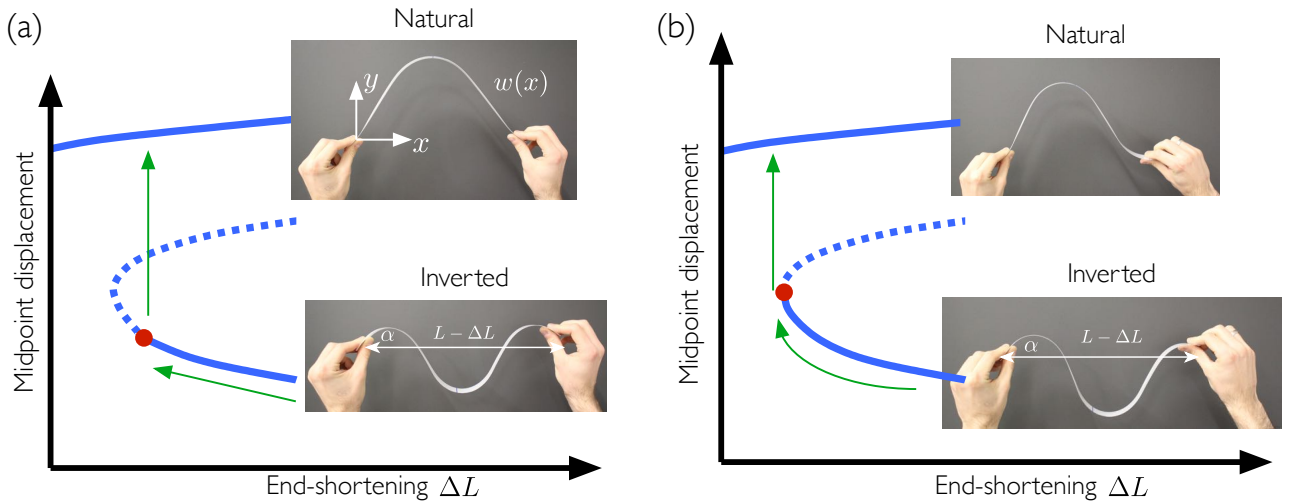


FIG. 1. Exploring ‘snap-through’ instabilities in a simple elastic system. (a) Bringing the edges of a strip of plastic together, while also holding them at a non-zero angle α to the horizontal, creates bistable ‘inverted’ (bottom) and ‘natural’ (top) arch shapes. Under smaller end-shortenings ΔL , the arch snaps from the inverted to the natural shape. Analysing the bifurcation behaviour shows that the instability underlying snapping in this case is a subcritical pitchfork bifurcation: the inverted mode (lower solid curve) intersects an unstable asymmetric mode (not drawn) at the point marked with a red dot; here it becomes linearly unstable (dashed curve). (Because the asymmetric mode is unstable it is not observed in practice.) (b) Introducing asymmetry in the boundary conditions, by holding the right end horizontally, still creates a bistable system. However, the destabilizing effect of the asymmetric mode is removed and the inverted mode remains stable up to a fold (indicated by the red dot): the snap-through bifurcation is now a saddle-node/fold bifurcation.

the early stages and the under-damped oscillations about the natural state. The inset of Fig. 3 shows that the displacement of the midpoint initially grows quadratically in time, in contrast to the exponential growth that is observed in systems at the onset of instability [6, 16]; a systematic slowing down is also seen in both the displacement and the snap-through time, t_{snap} (inset of Fig. 4), as the bifurcation point ΔL_{fold} is approached. This slowing down behaviour is reminiscent of critical slowing down in a number of physical phenomena [18–22].

To understand these observations, we analyse the linear beam equation, (1), incorporating the lateral confinement of the (inextensible) arch, which for small deflections is approximated by

$$\int_0^L \left(\frac{\partial w}{\partial x} \right)^2 dx = 2\Delta L. \quad (3)$$

The inclination angle α enters through the boundary condition $w_x(0, t) = \alpha$ (subscripts denote differentiation) while the other boundary conditions are homogeneous, $w(0, t) = w(L, t) = w_x(L, t) = 0$. The linearity of the beam equation (1) and the form of the confinement (3) show that w_x can be rescaled by $(\Delta L/L)^{1/2}$ and, using L as the natural horizontal length scale, we see immediately that a single dimensionless parameter emerges:

$$\mu = \alpha \left(\frac{\Delta L}{L} \right)^{-1/2}. \quad (4)$$

The purely geometrical parameter μ is the key control parameter in the problem and may be understood as the

ratio of the angle imposed by clamping, α , to that imposed by confinement, $(\Delta L/L)^{1/2}$.

An analysis of the equilibrium solutions of (1) subject to the constraint (3) and the appropriate boundary conditions allows the shape of the inverted arch to be determined analytically where it exists (see Supplementary Information for details). This analysis confirms that bistability of the inverted shape is lost at a saddle-node bifurcation where $\mu = \mu_{\text{fold}} \approx 1.782$; the bifurcation shape, $w_{\text{fold}}(x)$, and the associated (constant) compressive force, $PL^2/B = \tau_{\text{fold}}^2 \approx 57.55$, can also be found explicitly.

To analyse the dynamics just beyond the bifurcation point, i.e. for end-shortenings ΔL slightly smaller than ΔL_{fold} , we set $\mu = \mu_{\text{fold}} + \Delta\mu$ with $0 < \Delta\mu \ll 1$. Because no inverted equilibrium exists for $\Delta\mu > 0$, we exploit the fact that the midpoint displacement is initially the same as at the bifurcation, i.e. $w(L/2, 0) = w_{\text{fold}}(L/2)$. For small $\Delta\mu$, the initial shape of the strip is therefore ‘close’ to the bifurcation shape everywhere, $w(x, 0) \approx w_{\text{fold}}(x)$ for $0 < x < L$. Introducing dimensionless variables $X = x/L$, $W = w/(L\Delta L)^{1/2}$, $W_{\text{fold}} = w_{\text{fold}}/(L\Delta L)^{1/2}$, $\mathcal{T} = t/t_*$ and $\tau^2 = PL^2/B$ we then seek a series solution of the form

$$W(X, \mathcal{T}) = W_{\text{fold}}(X) + \Delta\mu^{1/2} W_p(X) A(\mathcal{T}), \quad (5)$$

$$\tau(\mathcal{T}) = \tau_{\text{fold}} + \Delta\mu^{1/2} A(\mathcal{T}). \quad (6)$$

We find that $W_p(X)$ is a spatial eigenfunction that can be determined analytically, while the temporal variation

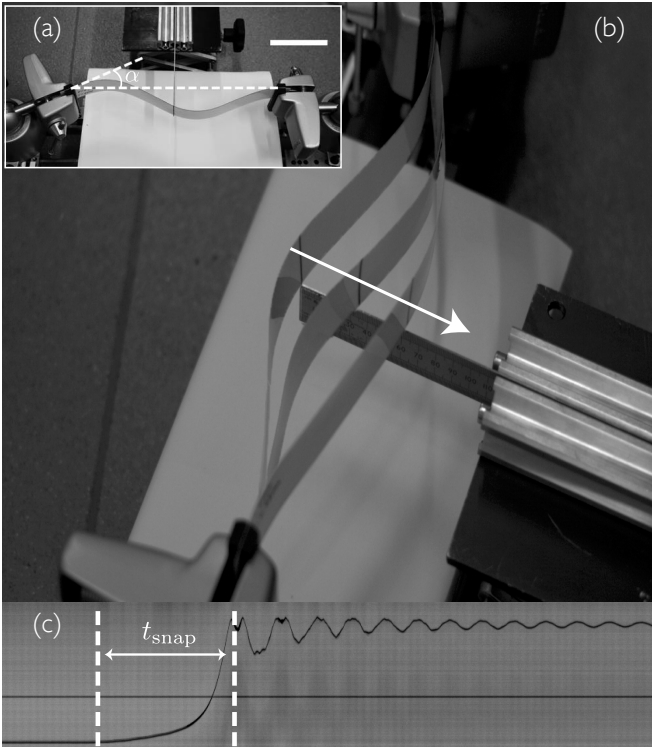


FIG. 2. Investigating the snapping dynamics of an elastic arch. (a) A thin strip is buckled into an unstable state with an end-shortening past the snapping transition, $\Delta L < \Delta L_{\text{fold}}$; a metal indenter prevents the strip from snapping by making contact at its midpoint and imposes $w(L/2, 0) = w_{\text{fold}}(L/2)$. Scale bar 10 cm. (b) The indenter is then lowered allowing the arch to snap (three successive stages superimposed). (See also Methods.) (c) A spatio-temporal plot of the midpoint reveals its trajectory during snapping (PET, $L = 240$ mm, $\alpha = 21.34^\circ$, $\Delta L_{\text{fold}} = 10.41$ mm, $w_{\text{fold}}(L/2) = -16.75$ mm, $\Delta L = 10.20$ mm). The montage begins before the point when the indenter loses contact with the strip, and ends as the arch oscillates about the natural shape (the horizontal line is at zero displacement). Slices through a total of 828 frames (separated by 1 ms) are shown.

of the motion, $A(\mathcal{T})$, satisfies

$$\Delta\mu^{-1/2} \frac{d^2 A}{d\mathcal{T}^2} = c_1 + c_2 A^2, \quad (7)$$

with $c_1 \approx 329.0$ and $c_2 \approx 417.8$ constants that depend on $W_p(X)$ and its integrals (see Supplementary Information).

The ordinary differential equation (7) represents a great simplification of the full system (1) and (3). Furthermore, (7) is generic for the dynamics of elastic snap-through without dissipation: the nonlinear term A^2 is inherited from the structure of the saddle-node bifurcation (the parabolic geometry near the fold) and should hold generically in inertial snap-through. With viscous damping, a similar analysis would lead to a single time derivative in (7). The specific details of the problem (e.g. boundary conditions) enter only through the constants c_1

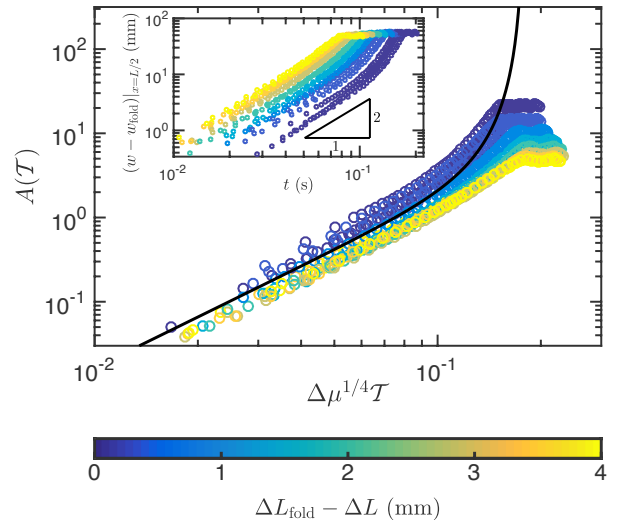


FIG. 3. Midpoint trajectories during snapping for different end-shortenings just beyond the snapping transition. Inset: Evolution of the midpoint position, $w(L/2, t)$, away from the initial value $w_{\text{fold}}(L/2)$ (PET, $L = 290$ mm, $\alpha = 19.85^\circ$, $\Delta L_{\text{fold}} = 9.20$ mm, $w_{\text{fold}}(L/2) = -20.95$ mm). For each value of $\Delta L_{\text{fold}} - \Delta L$ (given by the colour bar), three runs are recorded and shown here (circles). The time origin, $t = 0$, is the point where contact is first lost with the indenter (see Supplementary Information for details); data is plotted until the strip begins to oscillate about the natural shape. Main plot: The same data, rescaled in terms of the amplitude variable $A(\mathcal{T})$ as a function of dimensionless time $\mathcal{T} = t/t^*$. We see that while $A(\mathcal{T})$ remains small, the points collapse onto the predicted asymptotic behaviour (8) (solid black curve) with quadratic growth initially.

and c_2 .

Because the arch starts from rest at a shape close to the bifurcation shape, the appropriate initial conditions for (7) are $A(0) = A_{\mathcal{T}}(0) = 0$, giving the implicit solution

$$\Delta\mu^{1/4} \mathcal{T} = \sqrt{\frac{3}{2}} \int_0^{A(\mathcal{T})} \frac{d\xi}{(3c_1\xi + c_2\xi^3)^{1/2}}. \quad (8)$$

Expanding the right-hand side for $A \ll 1$, we obtain the asymptotic behaviour

$$A(\mathcal{T}) \sim \frac{c_1}{2} \Delta\mu^{1/2} \mathcal{T}^2,$$

when $\mathcal{T} \ll \Delta\mu^{-1/4}$. The initial growth of the midpoint displacement (and all other material points) is therefore ballistic, as observed experimentally (Fig. 3 inset); viscous dissipation would instead give $A \propto \mathcal{T}$. Furthermore, the full solution for $A(\mathcal{T})$ computed from (8) compares favourably to that observed experimentally while $A \lesssim 1$ (Fig. 3), with experimental data for different values of $\Delta\mu$ collapsing onto a single master curve. For $A \gg 1$ our asymptotic analysis breaks down and fails to predict how the strip approaches the natural equilibrium and oscillates; instead, the solution (8) blows up at time $\mathcal{T} = \mathcal{T}_b$

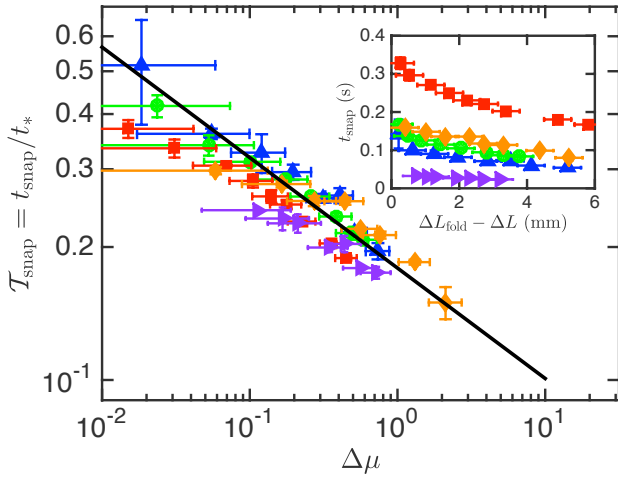


FIG. 4. Slowing down of snapping dynamics near the loss of bistability. Inset: The experimentally measured snapping time, t_{snap} (defined as the time taken to reach the first peak of vibrations, as labelled in Fig. 2c, averaged over three runs), as the end-shortening ΔL approaches the snapping threshold ΔL_{fold} from below. Data is shown for PET strips with $L = 240$ mm, $\alpha = 21.34^\circ$ (upward-pointing triangles), $L = 290$ mm, $\alpha = 19.85^\circ$ (circles) and $L = 430$ mm, $\alpha = 21.17^\circ$ (squares), as well as for experiments on steel strips with $L = 140$ mm, $\alpha = 22.51^\circ$ (right-pointing triangles) and 280 mm, $\alpha = 17.14^\circ$ (diamonds). Main plot: Snapping times, re-scaled by the inertial timescale t_* , as a function of the normalized distance to bifurcation $\Delta\mu = \mu - \mu_{\text{fold}}$ (computed from (4)). The data collapse onto the asymptotic prediction $\mathcal{T}_{\text{snap}} \approx 0.179\Delta\mu^{-1/4}$ from linear beam theory (solid black line). Horizontal error bars correspond to the uncertainties in measurements of α ($\pm 2^\circ$) and ΔL (± 200 μm) (see Methods); vertical error bars correspond to the standard deviation of the measured snapping times over three runs.

where

$$\mathcal{T}_b = \sqrt{\frac{3}{2}} \Delta\mu^{-1/4} \int_0^\infty \frac{d\xi}{(3c_1\xi + c_2\xi^3)^{1/2}} \approx 0.179\Delta\mu^{-1/4}. \quad (9)$$

This time therefore corresponds to the end of the ‘bottleneck phase’ in which the strip is influenced by its proximity to the inverted equilibrium at the fold. Because the motions are rapid by this stage, \mathcal{T}_b represents a natural approximation for the total snap-through time. The prediction (9) leads to a collapse of experimentally measured snapping times for strips composed of different materials

and natural lengths L , and predicts the dependence on $\Delta\mu$ well (Fig. 4).

The data in Fig. 4 and the expression for the snap-through time, (9), show that as the system approaches the snap-through transition the dynamics slow down significantly. This is characteristic of the dynamics near a bifurcation in a range of physical phenomena [19–23], which is commonly referred to as ‘critical slowing down’ [18], or as a ‘bottleneck’ due to the ‘ghost’ of the nearby equilibrium [24]. The importance of critical slowing down in elastic instabilities such as snap-through has not been appreciated previously, despite numerous previous experiments showing signs of diverging time scales as the threshold is approached [13, 14]. Furthermore, the inertial (rather than overdamped) dynamics here changes the exponents typically seen in critical slowing down ($\Delta\mu^{-1/4}$ rather than $\Delta\mu^{-1/2}$ [23]).

We note that the prefactor in the scaling $\mathcal{T}_b \sim \Delta\mu^{-1/4}$ depended on a detailed calculation and hence on the boundary conditions of the problem; here the prefactor is small, meaning that the snap-through time is comparable to the characteristic elastic time scale t_* for experimentally attainable $\Delta\mu$. However, in other systems the appropriate prefactor may be substantially larger and finer control of the distance to bifurcation $\Delta\mu$ may be possible; in such circumstances we expect that a substantial disparity between the observed snap-through time and the characteristic elastic time scale t_* may emerge. Biological systems such as the Venus flytrap may be particularly prone to such a slowing down, as the analogue of $\Delta\mu$ is often controlled by slow processes such as swelling or growth. In both biological and engineering settings, snap-through would seem to require a trade-off between the speed of snapping (a faster snap requiring larger $\Delta\mu$) and the time/energy taken to attain a large $\Delta\mu$. Critical slowing down may also mean that very close to the snap-through transition the system becomes overdamped (rather than inertial) leading to different scalings and slower dynamics; this possibility remains to be fully explored and may depend on the precise nature of the damping present (e.g. viscoelasticity in man-made applications [14] or poroelasticity in biological systems [7, 9]). Our analysis, combined with techniques for controlling snap-through such as solvent-induced swelling [25] or photo-initiation [26], may offer the possibility to tune the time scale of snap-through from fast to slow by controlling how far beyond the transition one takes the system.

-
- [1] Bazant, Z. & Cendolin, L. *Stability of Structures: Elastic, Inelastic, Fracture, and Damage Theories* (Oxford University Press, 1991).
- [2] Loh, O. Y. & Espinosa, H. D. Nanoelectromechanical contact switches. *Nature Nanotech.* **7**, 283–295 (2012).
- [3] Xu, P. *et al.* Unusual ultra-low-frequency fluctuations in freestanding graphene. *Nature Comm.* **5**, 3720 (2014).

- [4] Silverberg, J. L. *et al.* Origami structures with a critical transition to bistability arising from hidden degrees of freedom. *Nature Mat.* **14**, 389–393 (2015).
- [5] Dudte, L. H., Vouga, E., Tachi, T. & Mahadevan, L. Programming curvature using origami tessellations. *Nature Mater.* **15**, 583–588 (2016).
- [6] Pandey, A., Moulton, D. E., Vella, D. & Holmes, D. P.

- Dynamics of snapping beams and jumping poppers. *EPL* **105**, 24001 (2014).
- [7] Skotheim, J. M. & Mahadevan, L. Physical limits and design principles for plant and fungal movements. *Science* **308**, 1309–1310 (2005).
- [8] Forterre, Y. Slow, fast and furious: understanding the physics of plant movements. *J. Exp. Bio.* **64**, 4745–4760 (2013).
- [9] Forterre, Y., Skotheim, J. M., Dumais, J. & Mahadevan, L. How the Venus flytrap snaps. *Nature* **433**, 421–425 (2005).
- [10] Smith, M. L., Yanega, G. M. & Ruina, A. Elastic instability model of rapid beak closure in hummingbirds. *J. Theo. Bio.* **282**, 41–51 (2011).
- [11] Gonçalves, P. B. *et al.* Dynamic non-linear behavior and stability of a ventricular assist device. *Int. J. Solids Struct.* **40**, 5017–5035 (2003).
- [12] Daynes, S., Potter, K. & Weaver, P. M. Bistable pre-stressed buckled laminates. *Comp. Sci. Tech.* **68**, 3431–3437 (2010).
- [13] Hung, E. S. & Senturia, S. D. Generating efficient dynamical models for microelectromechanical systems from a few finite-element simulation runs. *J. MEMS* **8**, 280–289 (1999).
- [14] Brinkmeyer, A., Pirrera, A., Santer, M. & Weaver, P. M. Pseudo-bistable pre-stressed morphing composite panels. *Int. J. Solids Struct.* **50**, 1033–1043 (2013).
- [15] Plaut, R. H. & Virgin, L. N. Vibration and snap-through of bent elastica strips subjected to end rotations. *J. Appl. Mech.* **76**, 041011 (2009).
- [16] Fargette, A., Neukirch, S. & Antkowiak, A. Elastocapillary snapping: capillarity induces snap-through instabilities in small elastic beams. *Phys. Rev. Lett.* **112**, 137802 (2014).
- [17] Pippard, A. B. *Response and Stability* (Cambridge University Press, 1985).
- [18] Chaikin, P. M. & Lubensky, T. C. *Principles of Condensed Matter Physics* (Cambridge University Press, 2000).
- [19] Tredicce, J. R. *et al.* Critical slowing down at a bifurcation. *Am. J. Phys.* **72**, 799–809 (2004).
- [20] Strogatz, S. H. & Westervelt, R. M. Predicted power laws for delayed switching of charge-density waves. *Phys. Rev. B* **40**, 10501 (1989).
- [21] Dakos, V. *et al.* Slowing down as an early warning signal for abrupt climate change. *Proc. Natl Acad. Sci.* **105**, 14308–14312 (2008).
- [22] Scheffer, M. *et al.* Early-warning signals for critical transitions. *Nature* **461**, 53–59 (2009).
- [23] Aranson, I. S., Malomed, B. A., Pismen, L. M. & Tsimring, L. S. Crystallization kinetics and self-induced pinning in cellular patterns. *Phys. Rev. E* **62**, R5–R8 (2000).
- [24] Strogatz, S. H. *Nonlinear Dynamics and Chaos with Applications to Physics, Biology, Chemistry and Engineering* (Westview Press, Philadelphia, 2015).
- [25] Holmes, D. P. & Crosby, A. J. Snapping surfaces. *Adv. Mater.* **19**, 3589–3593 (2007).
- [26] Shankar, M. R. *et al.* Contactless, photoinitiated snap-through in azobenzene-functionalized polymers. *Proc. Natl. Acad. Sci.* **110**, 18792–18797 (2013).

ACKNOWLEDGMENTS

We are grateful to Jean-Baptiste Gorce for early experiments in a related system and to Jonathan Dawes, Sébastien Neukirch, and Jin-Chong Tan for discussions. The research leading to these results has received funding from the European Research Council under the European Union’s Horizon 2020 Programme / ERC Grant Agreement no. 637334 (DV) and the EPSRC Grant No. EP/M50659X/1 (MG).

SUPPLEMENTARY INFORMATION

Further detail on the theoretical analysis of the snapping problem and the experimental procedures is available in the Supplementary Information (appended).

DATA AVAILABILITY

The experimental data that supports the plots within this paper and other findings of this study are available from <http://dx.doi.org/10.5287/bodleian:RyGXnqJGk>.

METHODS

Sample preparation. Strips were prepared from biaxially oriented polyethylene terephthalate (PET) film (Goodfellow, Cambridge, $\rho_s = 1.337 \text{ g cm}^{-3}$, $h = 0.35 \text{ mm}$, $E = 5.707 \text{ GPa}$) and stainless steel rolled shim (304 grade, RS components, $\rho_s = 7.881 \text{ g cm}^{-3}$, $h = 0.1 \text{ mm}$, $E = 203.8 \text{ GPa}$). The value of the Young’s modulus E for each material were determined by analysing the frequency of small-amplitude vibrations of the strip. The time scale of snapping was varied by varying the length of the strip: for PET we used lengths $L \in \{240, 290, 430\} \text{ mm}$ while for steel we used $L \in \{140, 280\} \text{ mm}$. Experiments were conducted at room temperature, well below the glass transition temperature of PET, so that this material acts as a glassy polymer, showing little viscous creep and dynamic dissipation (see [27, 28] for example).

Snapping experiments. The ends of each strip are clamped into vice clamps (PanaVise 301) which are mounted onto a linear track so that the strip deforms in one plane only. To minimize the effect of gravity, the strip is oriented sideways so its width lies in the vertical direction (see Fig. 2a,b of the main text). The right clamp is fixed parallel to the track, while the left clamp holds the strip at an angle $\alpha \neq 0$ (constant throughout each experiment) and can be moved along the track to vary the applied end-shortening ΔL . A digital camera mounted above the left clamp allows α to be determined to an accuracy of $\pm 2^\circ$, and changes in ΔL to be measured to an accuracy of $\pm 200 \mu\text{m}$ (by measuring displacement of the clamp from a known reference state).

The snapping dynamics are filmed using a high speed camera (Phantom Miro 310) at a frame rate of 1000 fps. The camera is placed vertically above the strip, allowing the mid-point position (marked on the edge) to be recorded when the

strip is in equilibrium and during motion. Beyond the fold, i.e. when only one equilibrium exists, the strip is forced to start close to the fold shape using a metal ruler (tip width 1 mm) attached to a laboratory jack; this is then lowered

vertically out of contact with the strip to allow snapping to proceed. The resulting movie is cropped around the midpoint position and converted to a spatio-temporal plot (montage) of its trajectory using ImageJ (NIH).

[27] Shi, Y. & Jabarin, S. A. Glass-transition and melting behavior of poly(ethylene terephthalate)/poly(ethylene 2,6-naphthalate) blends. *J. Appl. Poly. Sci.* **81**, 11–22 (2001).

[28] Demirel, B. & Yaras, A. & Elçiçek, H. Crystallization behavior of PET materials. *BAÜ Fen Bil. Enst. Dergisi Cilt* **13**, 26–35 (2011).

Supplementary information for “Critical slowing down in purely elastic ‘snap-through’ instabilities”

This supplementary information gives further detail on the theoretical analysis of the snapping problem and the experimental procedures than is possible in the main text. In particular, §I discusses the use of linear beam theory to characterize the bistability of our system and the early-time dynamics of snap-through. In §II we discuss how we experimentally determine the location of the fold point and extract the midpoint trajectory from the movies of snapping.

I. THEORETICAL ANALYSIS

The transverse displacement of the strip, $w(x, t)$, is modelled using the linear dynamic beam equation [S5]

$$\rho_s h \frac{\partial^2 w}{\partial t^2} + B \frac{\partial^4 w}{\partial x^4} + P \frac{\partial^2 w}{\partial x^2} = 0, \quad 0 < x < L. \quad (\text{S1})$$

Here x is the horizontal coordinate (measured from the left end), t is time, and $P(t)$ is the (unknown) compressive force applied to the strip (per unit width). The properties of the strip are its natural length L , thickness h , density ρ_s , and bending stiffness $B = Eh^3/12$ (with E the Young’s modulus). (Note that we use the bending stiffness appropriate for a narrow strip, see [S2].)

The left end of the strip is clamped at an inclination angle $0 < \alpha \ll 1$, while the right end is clamped horizontally. This corresponds to the boundary conditions (here and throughout subscripts denote partial derivatives)

$$w(0, t) = 0, \quad w_x(0, t) = \alpha, \quad w(L, t) = w_x(L, t) = 0. \quad (\text{S2})$$

We consider slender strips, $h \ll L$, well beyond the buckling threshold so that the extensibility of the strip may be neglected (see [S8] for a discussion of this in a related problem). The lateral confinement of the strip then becomes $\int_0^L \cos \theta \, ds = L - \Delta L$ where $\theta(s, t)$ is the angle made by the strip to the horizontal, s is the arclength and ΔL is the imposed end-shortening. Using the assumption of small slopes implicit in the beam equation, we identify $s \sim x$ and $\theta \sim w_x \ll 1$ so this is approximated as

$$\int_0^L \left(\frac{\partial w}{\partial x} \right)^2 dx = 2\Delta L. \quad (\text{S3})$$

Equation (S1) with boundary conditions (S2), the constraint (S3) and initial conditions fully specify the problem. We take as initial conditions zero initial velocity, $w_t(x, 0) = 0$, and initial shape $w(x, 0) = w_0(x)$, where the function $w_0(x)$ shall be specified later.

A. Non-dimensionalization

To make the problem dimensionless, we scale the horizontal coordinate by the length L of the strip, i.e we set $X = x/L$. Balancing terms in the inextensibility constraint (S3) shows that a typical slope $w_x \sim (\Delta L/L)^{1/2}$, giving the natural vertical length scale $w \sim (L\Delta L)^{1/2}$. We therefore introduce the dimensionless displacement $W = w/(L\Delta L)^{1/2}$. Time is scaled as $\mathcal{T} = t/t_*$ where $t_* = (\rho_s h L^4/B)^{1/2}$ is the inertial time scale (obtained by balancing inertial and bending forces in (S1)). Inserting these scalings into the beam equation (S1), we obtain

$$\frac{\partial^2 W}{\partial \mathcal{T}^2} + \frac{\partial^4 W}{\partial X^4} + \tau^2 \frac{\partial^2 W}{\partial X^2} = 0, \quad 0 < X < 1, \quad (\text{S4})$$

where $\tau(\mathcal{T})^2 = PL^2/B$ is the dimensionless compressive force.

With this non-dimensionalization, the constraint (S3) becomes

$$\int_0^1 \left(\frac{\partial W}{\partial X} \right)^2 dX = 2, \quad (\text{S5})$$

while the boundary conditions (S2) are modified to

$$W_X(0, \mathcal{T}) = \mu \equiv \alpha(\Delta L/L)^{-1/2}, \quad W(0, \mathcal{T}) = W(1, \mathcal{T}) = W_X(1, \mathcal{T}) = 0. \quad (\text{S6})$$

Together with appropriate initial conditions for W and $W_{\mathcal{T}}$, these equations provide a closed system to determine the profile $W(X, \mathcal{T})$ and compressive force $\tau(\mathcal{T})^2$.

By non-dimensionalizing the problem we have reduced the control parameters α and ΔL to the single parameter μ , which enters the problem as a normalized inclination angle (the dimensionless compressive force τ^2 acts as a Lagrange multiplier and is determined as part of the solution). The parameter μ measures the ratio of the angle imposed by clamping, α , to that due to the imposed end-shortening, $(\Delta L/L)^{1/2}$, and so is entirely geometric in nature; it is independent of the material parameters of the system, notably ρ_s and E (and also the thickness h). While the combination of parameters encapsulated in μ has been identified empirically before [S3], the analytical understanding here is, to our knowledge, new. Finally, we note that μ is the ratio of bending energy to stretching energy within the strip and, as such, is the analogue of the Föppl-von-Kármán number γ for shallow spherical caps [S4].

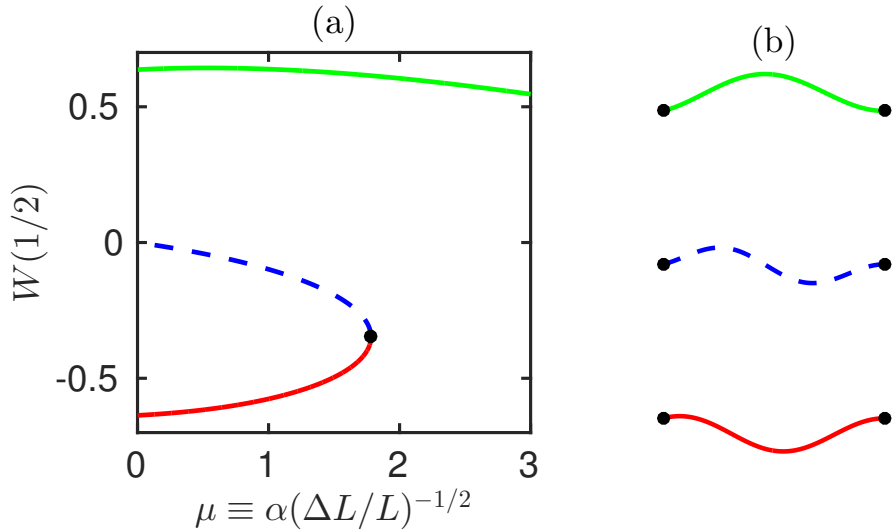


FIG. S1. The equilibrium behaviour of the strip, as predicted by linear beam theory. (a) Bifurcation diagram: plotting the dimensionless midpoint displacement as a function of $\mu = \alpha(\Delta L/L)^{-1/2}$. The upper branch (solid green curve) corresponds to the ‘natural’ shape, while the lower branch (solid red curve) corresponds to the ‘inverted’ shape that disappears at the saddle-node (fold) bifurcation at $\mu \approx 1.7818$. (b) The corresponding strip shapes, $W(X)$, for each of these modes when $\mu = 1$.

B. Equilibrium shapes

The solution of the static beam equation (S4) subject to the boundary conditions (S6) is

$$W(X) = \mu \frac{\tau X(\cos \tau - 1) + \tau[\cos \tau(1 - X) - \cos \tau] - \sin \tau X - \sin \tau(1 - X) + \sin \tau}{\tau(2 \cos \tau + \tau \sin \tau - 2)}. \quad (\text{S7})$$

To determine τ in terms of the control parameter μ , we substitute (S7) into the end-shortening constraint (S5) and rearrange to find

$$\mu^2 = \frac{8\tau(2 \cos \tau + \tau \sin \tau - 2)^2}{2\tau^3 - \tau^2(\sin 2\tau + 4 \sin \tau) + 4\tau(\cos \tau - \cos 2\tau) + 2(\sin 2\tau - 2 \sin \tau)}. \quad (\text{S8})$$

For each value of μ , the allowed values of $\tau(\mu)$ may be found numerically (e.g. using the MATLAB routine `fsolve`). Because τ does not manifest itself experimentally, we plot the resulting bifurcation diagram in terms of $W(1/2)$ and μ , using

$$W(1/2) = \mu \frac{\tan(\tau/4)}{2\tau}, \quad (\text{S9})$$

which follows from (S7). This result is shown in figure S1, and confirms that the ‘inverted’ equilibrium shape (the red branch in figure S1) undergoes a saddle-node (fold) bifurcation when

$$\mu = \mu_{\text{fold}} \approx 1.7818, \quad W(1/2) = W_{\text{fold}}(1/2) \approx -0.3476, \quad \tau = \tau_{\text{fold}} \approx 7.5864.$$

Note that it can be shown via standard techniques (see [S7], for example), that the branches represented by solid curves in figure S1 are stable, while that represented by a blue dashed curve is unstable.

If the clamp angle α is fixed and μ is varied by changing the end-shortening ΔL (as in our experiments), the snapping bifurcation occurs at

$$\Delta L_{\text{fold}} \approx 0.315\alpha^2 L.$$

C. Dynamics of snap-through

We now analyse the situation in which the system is placed just beyond the saddle-node bifurcation, i.e. we set $\mu = \mu_{\text{fold}} + \Delta\mu$ with $0 < \Delta\mu \ll 1$, a small perturbation. Because no inverted equilibrium exists for $\Delta\mu > 0$ (i.e. we are to the right of the fold point in figure S1), it follows that for the strip to reach an equilibrium, it must snap upwards to the natural shape.

We take an initial condition that is ‘close’ to the shape of the arch at the fold bifurcation, i.e. $W(X, 0) \approx W_{\text{fold}}(X)$. (Experimentally this condition is imposed by the indenter, which fixes the midpoint position to be that taken at bifurcation; away from the midpoint $W(X, 0) \approx W_{\text{fold}}(X)$ then holds because $\Delta L \approx \Delta L_{\text{fold}}$ for $\Delta\mu \ll 1$). For $\Delta\mu$ sufficiently small, we

expect that the shape of the snapping beam will only evolve away from $W_{\text{fold}}(X)$ on a time scale that is much slower than the inertial time scale of the beam — we have that $W(X, \mathcal{T}) \approx W_{\text{fold}}(X)$ (and also $\tau \approx \tau_{\text{fold}}$) up to some dimensionless time $\mathcal{T} \gg 1$. To capture this explicitly we rescale time as $T = \Delta\mu^\eta \mathcal{T}$, where $\eta > 0$ characterizes the duration of this slow ‘bottleneck’ phase and will be determined as part of the analysis. In terms of scaled variables, the beam equation (S4) reads

$$\Delta\mu^{2\eta} \frac{\partial^2 W}{\partial T^2} + \frac{\partial^4 W}{\partial X^4} + \tau^2 \frac{\partial^2 W}{\partial X^2} = 0, \quad 0 < X < 1. \quad (\text{S10})$$

We now seek a series solution about the bifurcation shape of the form

$$W(X, T) = W_{\text{fold}}(X) + \Delta\mu^{1/2} W_0(X, T) + \Delta\mu W_1(X, T) + \dots, \quad (\text{S11})$$

$$\tau(T) = \tau_{\text{fold}} + \Delta\mu^{1/2} \tau_0(T) + \Delta\mu \tau_1(T) + \dots \quad (\text{S12})$$

The choice of powers of $\Delta\mu^{1/2}$ can be justified *a posteriori* and reflects the fact that the displacement (away from the bifurcation shape) in the bottleneck is much larger than the original perturbation to the system, $\Delta\mu$. A similar scaling also arises in bottleneck phenomena near the pattern forming threshold in the Swift-Hohenberg equation [S1].

1. Leading-order problem

Inserting (S11)–(S12) into (S10) and considering terms of $O(\Delta\mu^{1/2})$, we obtain the homogeneous equation

$$L(W_0, \tau_0) \equiv \frac{\partial^4 W_0}{\partial X^4} + \tau_{\text{fold}}^2 \frac{\partial^2 W_0}{\partial X^2} + 2\tau_{\text{fold}} \tau_0 \frac{d^2 W_{\text{fold}}}{dX^2} = 0. \quad (\text{S13})$$

The end-shortening constraint (S5) and boundary conditions (S6) are also homogeneous at $O(\Delta\mu^{1/2})$:

$$\int_0^1 \frac{dW_{\text{fold}}}{dX} \frac{\partial W_0}{\partial X} dX = 0, \quad W_0(0, T) = W_{0,X}(0, T) = W_0(1, T) = W_{0,X}(1, T) = 0.$$

Because the leading-order problem is homogeneous, it is equivalent to the equations governing small-amplitude oscillations about the bifurcation shape $(W_{\text{fold}}, \tau_{\text{fold}})$ restricted to neutrally stable (‘slow’) eigenmodes whose natural frequency (eigenvalue) is zero. Using linearity of the operator $L(\cdot, \cdot)$, we may scale τ_0 out from (S13) (since τ_0 is independent of X) so that

$$(W_0, \tau_0) = A(T)(W_p(X), 1). \quad (\text{S14})$$

Here $A(T)$ is an (undetermined) amplitude and $W_p(X)$ is the eigenmode satisfying equation (S13) with $\tau_0 = 1$, i.e.

$$L(W_p, 1) = 0, \quad \int_0^1 \frac{dW_{\text{fold}}}{dX} \frac{dW_p}{dX} dX = 0, \quad (\text{S15})$$

$$W_p(0) = \left. \frac{dW_p}{dX} \right|_{X=0} = W_p(1) = \left. \frac{dW_p}{dX} \right|_{X=1} = 0. \quad (\text{S16})$$

While this system appears to over-determine $W_p(X)$ (there are four derivatives but five constraints), there is in fact a unique solution

$$W_p(X) = \frac{1}{\tau_{\text{fold}}} \left(X \frac{dW_{\text{fold}}}{dX} - \mu_{\text{fold}} X \right) + a_1 (\sin \tau_{\text{fold}} X - \tau_{\text{fold}} X) + a_2 (\cos \tau_{\text{fold}} X - 1), \quad (\text{S17})$$

where

$$a_1 = -2\mu_{\text{fold}} \frac{\sin^2(\tau_{\text{fold}}/2) [(\tau_{\text{fold}}^2 - 2) \cos \tau_{\text{fold}} - 2\tau_{\text{fold}} \sin \tau_{\text{fold}} + 2]}{\tau_{\text{fold}}^2 (2 \cos \tau_{\text{fold}} + \tau_{\text{fold}} \sin \tau_{\text{fold}} - 2)^2},$$

and

$$a_2 = -\mu_{\text{fold}} \frac{\tau_{\text{fold}}^3 + \tau_{\text{fold}}^2 \sin \tau_{\text{fold}} (\cos \tau_{\text{fold}} - 2) + 2(\tau_{\text{fold}} \cos \tau_{\text{fold}} - \sin \tau_{\text{fold}})(\cos \tau_{\text{fold}} - 1)}{\tau_{\text{fold}}^2 (2 \cos \tau_{\text{fold}} + \tau_{\text{fold}} \sin \tau_{\text{fold}} - 2)^2}.$$

(This solution is found by applying the boundary conditions (S16), but also satisfies (S15) since, by construction, τ_{fold} is the value of τ taken at the fold.)

Subsequently, we shall need two integrals associated with (S17); we record the values of these integrals here:

$$I_1 = \int_0^1 W_p^2 dX \approx 0.0518, \quad I_2 = \int_0^1 \left(\frac{dW_p}{dX} \right)^2 dX \approx 0.950. \quad (\text{S18})$$

The variable $A(T)$ appearing in (S14) plays a key role in the snapping dynamics, because it acts as an amplitude of the leading-order solution (and also its compressive force). More explicitly, re-arranging the original series expansion in (S11) shows that

$$A(T) \sim \Delta\mu^{-1/2} \frac{W(X, T) - W_{\text{fold}}(X)}{W_p(X)}.$$

The amplitude $A(T)$ therefore characterizes how the strip evolves away from the bifurcation shape during the bottleneck phase. Currently, $A(T)$ is undetermined. We proceed to the next order problem to determine $A(T)$.

2. First-order problem

The amplitude $A(T)$ will be determined by a solvability condition on the first-order problem. In order to obtain dynamics at leading order, i.e. for A to be a non-constant function of time, the inertia term must come into play at $O(\Delta\mu)$, which requires $\eta = 1/4$. With this choice, at $O(\Delta\mu)$ the beam equation (S10) becomes

$$L(W_1, \tau_1) = -W_p \frac{d^2 A}{dT^2} - A^2 \left(2\tau_{\text{fold}} \frac{d^2 W_p}{dX^2} + \frac{d^2 W_{\text{fold}}}{dX^2} \right). \quad (\text{S19})$$

The end-shortening constraint (S5) and boundary conditions (S6) at $O(\Delta\mu)$ have the form

$$\int_0^1 \frac{dW_{\text{fold}}}{dX} \frac{\partial W_1}{\partial X} dX = -\frac{1}{2} A^2 \int_0^1 \left(\frac{dW_p}{dX} \right)^2 dX = -\frac{1}{2} I_2 A^2, \\ \frac{dW_1}{dX} \Big|_{X=0} = 1, \quad W_1(0, T) = W_1(1, T) = \frac{dW_1}{dX} \Big|_{X=1} = 0.$$

3. Solution for $A(T)$

Equation (S19) features the same linear operator $L(\cdot, \cdot)$ as in the leading-order problem, but now with an inhomogeneous right-hand side. The Fredholm Alternative Theorem [S6] implies that solutions exist only for a certain right-hand side, yielding a solvability condition that takes the form of an ODE for $A(T)$. We formulate this condition in the usual way: we multiply (S19) by the solution of the homogeneous adjoint problem, integrate over the domain, and use integration by parts to shift the operator onto the adjoint solution. In this case, the operator $L(\cdot, \cdot)$ is self-adjoint and so a solution of the homogeneous adjoint problem is simply $W_p(X)$. Performing these steps and simplifying (making use of the various boundary conditions that W_{fold} , W_p and W_1 satisfy) leads to

$$\frac{d^2 A}{dT^2} = c_1 + c_2 A^2, \quad (\text{S20})$$

where

$$c_1 = \frac{4\tau_{\text{fold}}}{\mu_{\text{fold}} I_1} \approx 329.0, \quad c_2 = \frac{3\tau_{\text{fold}} I_2}{I_1} \approx 417.8, \quad (\text{S21})$$

where the integrals I_1 and I_2 are as defined in (S18). (Note that due to the scaled time $T = \Delta\mu^{1/4} \mathcal{T}$, this differs slightly to the amplitude equation (7) given in the main text.)

Similar analyses have previously been performed for over-damped dynamics in the Swift–Hohenberg equation [S1], leading to the over-damped version of (S20), i.e. with the second derivative on the left-hand side replaced by a first derivative. The overdamped version of (S20) is well known as the canonical form of the dynamics close to a saddle-node bifurcation [S9] and is, in turn, known to give rise to a bottleneck whose duration diverges as the bifurcation point is approached. We shall see that (S20) exhibits a similar bottleneck phenomenon but emphasize that the dynamics here is purely inertial: there is no dissipation in our model.

To solve (S20), we need initial conditions for A and A_T . Because μ is perturbed by an amount $\Delta\mu$ from the fold point, it follows that $W(X, 0)$ (the initial shape of the strip under the indenter) agrees with $W_{\text{fold}}(X)$ to within $O(\Delta\mu)$. (Alternatively, the steady indentation problem can be solved to obtain the shape of the beam, $W_{\text{indent}}(X)$; comparing this with the bifurcation shape confirms that $|W_{\text{indent}}(X) - W_{\text{fold}}(X)| = O(\Delta\mu)$.) The leading-order part enters the series solution in (S11) at $O(\Delta\mu^{1/2})$ ($\gg \Delta\mu$), so that the initial conditions on A are homogeneous, i.e.

$$A(0) = A_T(0) = 0. \quad (\text{S22})$$

The scaling $T = \Delta\mu^{1/4} \mathcal{T}$ confirms the assumption that the bottleneck regime extends up to $\mathcal{T} \gg 1$. As (S20) is an $O(1)$ equation for $A(T)$ (ignoring numerical factors), the bottleneck time scales as

$$\mathcal{T} \sim \Delta\mu^{-1/4} \gg 1.$$

In fact, we can evaluate the bottleneck time directly. Multiplying (S20) by A_T and integrating twice (taking the positive root for A_T) we obtain the full solution implicitly:

$$T = \sqrt{\frac{3}{2}} \int_0^{A(T)} \frac{d\xi}{(3c_1 \xi + c_2 \xi^3)^{1/2}}. \quad (\text{S23})$$

As well as showing that $A(T)$ grows quadratically at early times, this solution also predicts that $A \rightarrow \infty$ in a finite time

$$T_b = \sqrt{\frac{3}{2}} \int_0^\infty \frac{d\xi}{(3c_1 \xi + c_2 \xi^3)^{1/2}} = \left(\frac{64\pi^2 c_1 c_2}{3} \right)^{-1/4} \Gamma\left(\frac{1}{4}\right)^2 \approx 0.179,$$

or, expressed in the dimensionless but unscaled time \mathcal{T} ,

$$\mathcal{T}_b \approx 0.179\Delta\mu^{-1/4}.$$

This blow-up corresponds to the end of the bottleneck regime — the strip is no longer influenced by its proximity to the bifurcation shape, and is rapidly accelerating upward to the natural mode. Expanding the right-hand side of (S23) shows that the strip accelerates out of the bottleneck according to the power law

$$A(T) \sim \frac{6}{c_2}(T_b - T)^{-2}.$$

Returning to our original series (S11)–(S12), we see that the perturbation variables are no longer small as soon as $A(T)$ grows to $O(\Delta\mu^{-1/2})$ and hence the amplitude equation (S20) is no longer asymptotically valid. Nevertheless, our treatment here allows us to obtain the key quantity of interest, the snapping time, which is dominated by the time spent getting through the bottleneck.

II. EXPERIMENTAL METHODS

A. Determining the snapping transition

The strip is first placed in the inverted equilibrium with a large enough end-shortening, ΔL , so that the system is bistable. We then decrease ΔL quasi-statically in small steps, measuring the midpoint displacement, $w(L/2)$, until the strip snaps. The dimensional bifurcation diagram obtained in this way is shown in figure S2a.

The bifurcation point, ΔL_{fold} , is never observed exactly: when we decrease ΔL , we introduce perturbations that cause snap-through slightly before the fold is reached. We determine ΔL_{fold} by fitting the data points close to the transition to a parabola (dotted curves in figure S2a) — the generic form expected close to the fold. This best-fit parabola also predicts the corresponding midpoint position at the bifurcation point, $w_{\text{fold}}(L/2)$, which is then the midpoint displacement fixed by the indenter. Note that this fitting procedure only needs to be performed once for each strip.

In determining the bifurcation diagram experimentally, various errors are introduced in the measurement of the angle α and the end-shortening ΔL . To plot the dimensionless bifurcation diagram (figure S2b) we therefore allow the value of α to vary (within the limits of experimental uncertainty, $\pm 2^\circ$) so that the experimentally determined fold point is as close as possible to that predicted theoretically. The result, plotted in terms of $\mu = \alpha(\Delta L/L)^{-1/2}$, is compared with the result of the linear beam theory in figure S2b. The fitted position of the fold, μ_{fold} (as predicted from the best-fit parabola), is displayed in each case (dotted vertical lines). Because the snapping dynamics depend sensitively on the size of $\Delta\mu = \mu - \mu_{\text{fold}}$, the theoretical value of μ_{fold} (≈ 1.7818) is not used to calculate $\Delta\mu$; instead, we use the shifted values of α , and the corresponding fitted values of μ_{fold} , since this is consistent with the observed behaviour of the strip prior to snapping. From here on, and throughout the main text, we refer to the shifted value of α for each experiment.

B. Extracting the midpoint trajectory

For values $\Delta L < \Delta L_{\text{fold}}$ (or equivalently $\mu > \mu_{\text{fold}}$), the strip snaps upward to the natural shape once contact with the indenter is lost. Each snapping movie begins before the moment at which the indenter loses contact; after converting this to a spatio-temporal plot (montage) of the midpoint position, the trajectory is therefore initially flat on the montage and it is not clear from these plots *when* the snapping motion first occurs. This start of the motion is key to the snapping time, and so this point must be determined by a fitting procedure.

The values of $w(L/2, t_{\text{raw}})$ are determined from the montage, with t_{raw} denoting the raw time (measured from the arbitrary start of the montage). Figure S3a shows a typical set of trajectories obtained in this way for snap-through at different values of $\Delta L < \Delta L_{\text{fold}}$; these are plotted in terms of the change in midpoint position away from the value imposed by the indenter, $\Delta w_{\text{mid}} \equiv (w - w_{\text{fold}})|_{x=L/2}$. Even without the moment of release determined, a semi-log plot of Δw_{mid} would reveal a straight line if the initial growth of the instability were exponential (as predicted by conventional stability analysis). This plot (figure S3b) does not indicate such an exponential growth.

If we instead assume power-law growth of the form

$$\Delta w_{\text{mid}} \propto (t_{\text{raw}} - t_0)^\beta, \tag{S24}$$

where t_0 is the time when contact is first lost and β is an (unknown) exponent (assumed positive), then

$$\frac{t_{\text{raw}} - t_0}{\beta} = \left\{ \frac{d}{dt_{\text{raw}}} \log \Delta w_{\text{mid}} \right\}^{-1}. \tag{S25}$$

A plot of the experimentally determined RHS of (S25) as a linear function of t_{raw} is shown in figure S4a. Despite the noise in the plot (which is due to numerical differentiation of the logarithm of our experimental data, as in (S25)), we see that our data is entirely consistent with $\beta = 2$, i.e. the strip deflection grows quadratically in time.

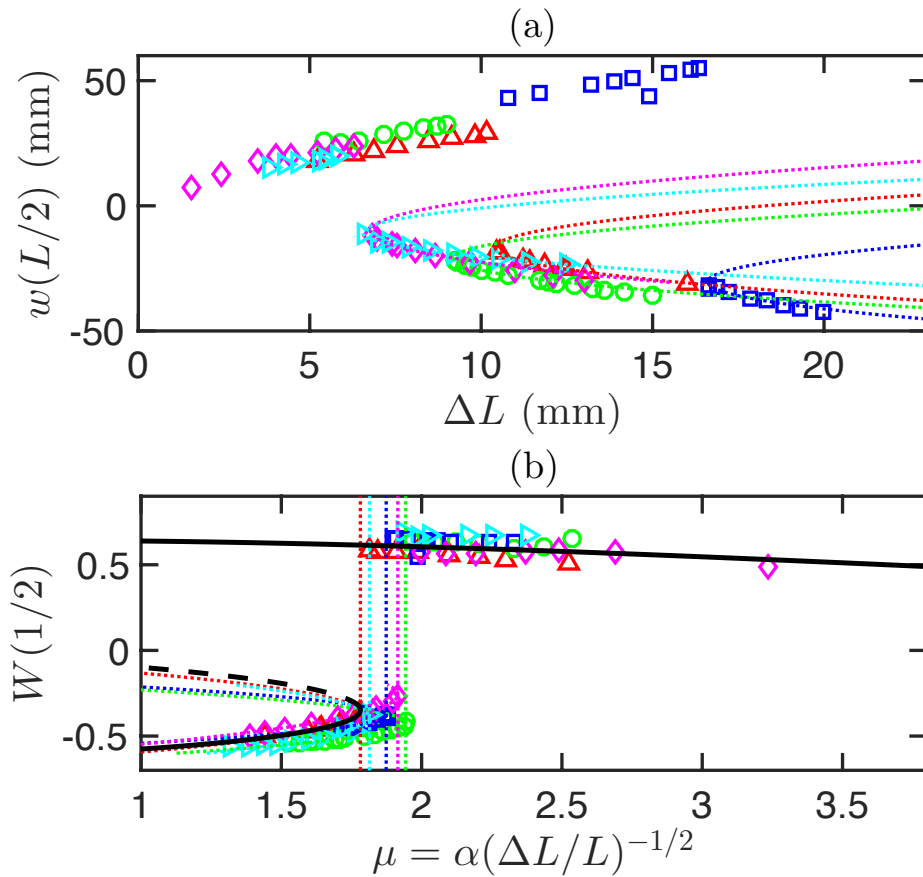


FIG. S2. (a) Midpoint position of equilibrium shapes as a function of the applied end-shortening, ΔL . Data is shown for PET strips with $L = 240$ mm (red upward-pointing triangles), $L = 290$ mm (green circles) and $L = 430$ mm (blue squares). Also plotted is data for steel strips with $L = 140$ mm (cyan right-pointing triangles) and $L = 280$ mm (magenta diamonds). The lower branches (i.e. with $w(L/2) < 0$) correspond to the ‘inverted’ shape while the upper branches (i.e. with $w(L/2) > 0$) correspond to the ‘natural’ shape after snap-through has occurred. In each case the best-fit (least-squares) parabola through the 6 points closest to the snapping transition is shown (dotted curves). (b) The same data plotted in dimensionless terms, where α has been chosen within the range of experimental uncertainty ($\pm 2^\circ$) so that the fitted bifurcation points (vertical dotted lines) are close to the theoretical value $\mu_{\text{fold}} \approx 1.7818$. The final points are $\mu_{\text{fold}} \approx 1.7884$, $\alpha = 21.34^\circ$ (red upward-pointing triangles), $\mu_{\text{fold}} \approx 1.9452$, $\alpha = 19.85^\circ$ (green circles), $\mu_{\text{fold}} \approx 1.8800$, $\alpha = 21.17^\circ$ (blue squares), $\mu_{\text{fold}} \approx 1.8174$, $\alpha = 22.51^\circ$ (cyan right-pointing triangles), and $\mu_{\text{fold}} \approx 1.9236$, $\alpha = 17.14^\circ$ (magenta diamonds). The prediction from linear beam theory (reproduced from figure S1a) is also shown (solid black curves).

A further check that the growth is quadratic is to plot the square root of the midpoint displacement as a function of t_{raw} on linear axes (figure S4b). This confirms a linear behaviour at early times, and allows us to determine the start of the snap, t_0 , from the intercept of the best-fit line with the horizontal axis. (We use the plotting procedure indicated in figure S4b to determine t_0 because this is less susceptible to noise than the approach used in figure S4a.)

In the main text, the dimensionless midpoint trajectories are plotted in terms of the amplitude $A(\mathcal{T})$, which is defined in the main text and implicitly via (S11) and (S14) to be

$$A(\mathcal{T}) = \frac{W(1/2, \mathcal{T}) - W_{\text{fold}}(1/2)}{\Delta\mu^{1/2}W_p(1/2)}. \quad (\text{S26})$$

In determining A , we use the value $W_p(1/2) \approx 0.3324$ determined from (S17). Figure S5 shows the experimentally determined $A(\mathcal{T})$ that were not shown in figure 3 of the main text; these experiments were performed with other lengths L and strips made of either PET or steel.

The results in figure S5 show that there is a reasonable collapse of experimental data with different values of ΔL onto a single curve for $A(\mathcal{T})$. However, we note that there is some dispersion of the data about the numerically predicted $A(\mathcal{T})$. We attribute this dispersion to uncertainty in the measured value of ΔL ($\pm 200 \mu\text{m}$), which increases the relative error in $\Delta\mu$ as

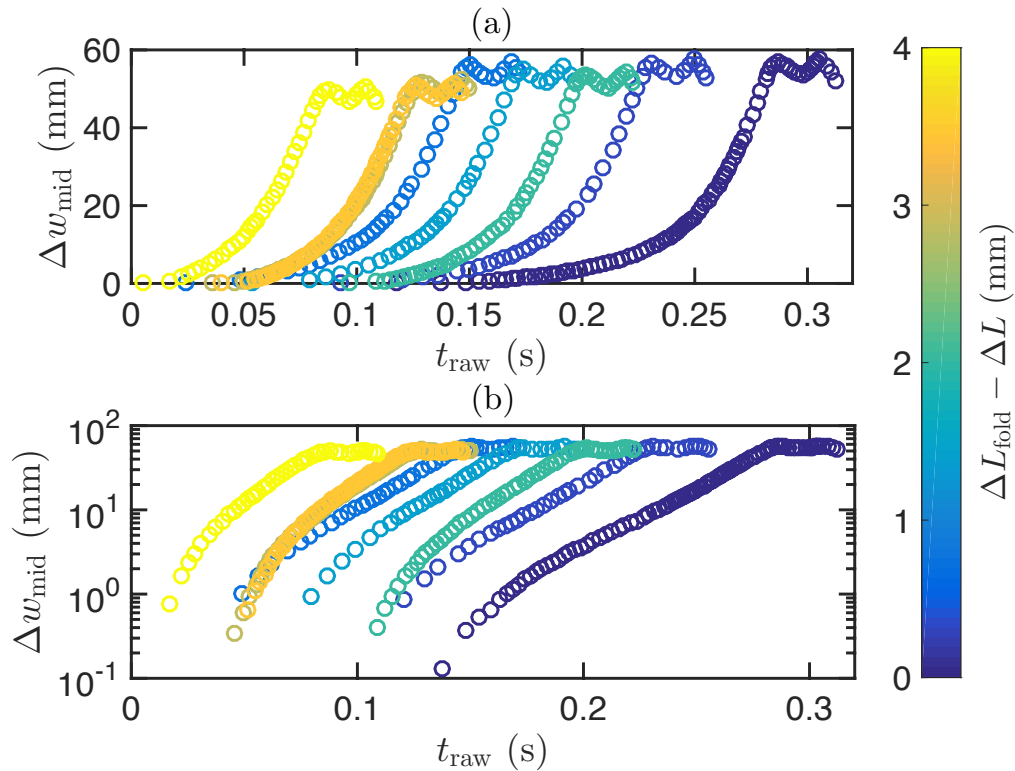


FIG. S3. Midpoint trajectories during snap-through measured at different end-shortenings beyond the snapping transition (PET, $L = 290$ mm, $\alpha = 19.85^\circ$, $\Delta L_{\text{fold}} = 9.20$ mm, $w_{\text{fold}}(L/2) = -20.95$ mm). (a) Evolution of the midpoint displacement from its initial value, $\Delta w_{\text{mid}} = (w - w_{\text{fold}})|_{x=L/2}$. For each end-shortening (given by colour bar), the snapping motion begins at some time $t_{\text{raw}} = t_0 > 0$ that is not known. (Note that data is plotted only until the strip begins to oscillate about the natural shape). (b) The same data plotted on semi-log axes do not suggest the presence of a classical linear instability in the initial motion (which would be indicated by a phase of exponential growth).

$\Delta L \rightarrow \Delta L_{\text{fold}}$.

-
- [S1] I. S. Aranson, B. A. Malomed, L. M. Pismen, and L. S. Tsimring. Crystallization kinetics and self-induced pinning in cellular patterns. *Phys. Rev. E*, 62(1):R5, 2000.
- [S2] B. Audoly and Y. Pomeau. *Elasticity and geometry: from hair curls to the non-linear response of shells*. Oxford University Press, 2010.
- [S3] A. Brinkmeyer. *Time-dependent Bistable Morphing Structures*. PhD thesis, University of Bristol, 2014.
- [S4] G. W. Brodland and H. Cohen. Deflection and snapping of spherical caps. *Int. J. Solids Struct.*, 23(10):1341, 1987.
- [S5] P. Howell, G. Kozyreff, and J. Ockendon. *Applied Solid Mechanics*. Cambridge University Press, Cambridge, 2009.
- [S6] J. P. Keener. *Principles of Applied Mathematics*. Addison-Wesley, Redwood City, 1988.
- [S7] J. H. Maddocks. Stability and folds. *Arch. Rational Mech. Anal.*, 99(4):301, 1987.
- [S8] A. Pandey, D. E. Moulton, D. Vella, and D. P. Holmes. Dynamics of snapping beams and jumping poppers. *EPL*, 105(2):24001, 2014.
- [S9] S. H. Strogatz. *Nonlinear Dynamics and Chaos with Applications to Physics, Biology, Chemistry and Engineering*. Westview Press, Philadelphia, 2015.

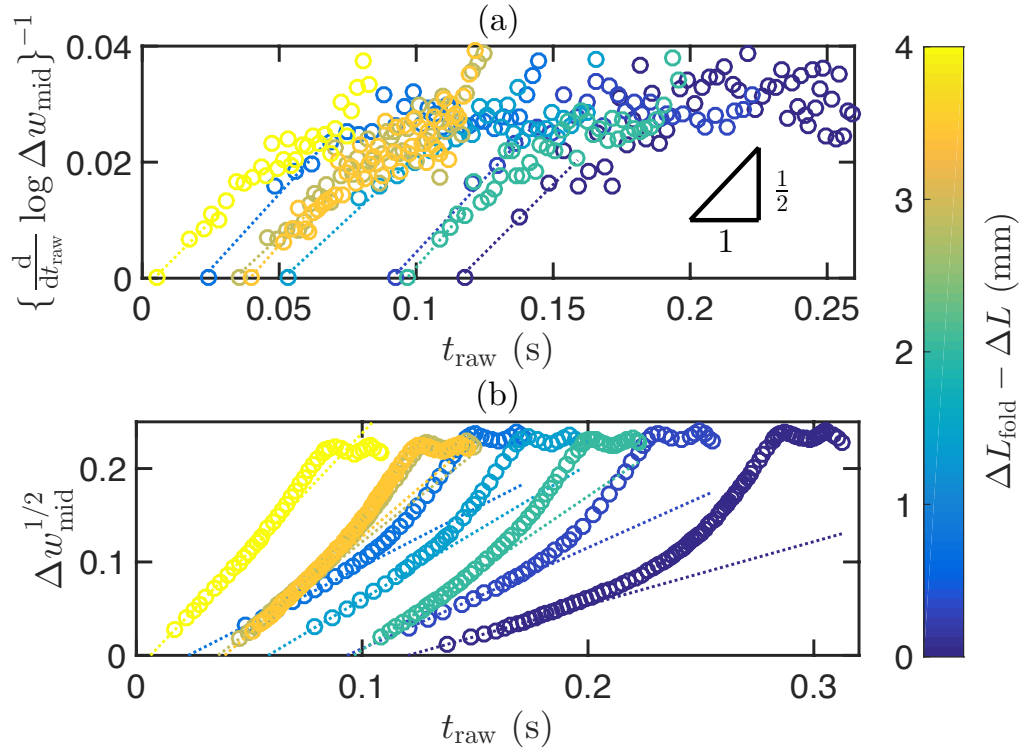


FIG. S4. (a) The same data in figure S3 rescaled according to the right-hand side of (S25) (numerical differentiation was performed using forward differences). A linear (least-squares) fit over the first 5 points in each case (dotted lines) gives the estimates $\beta \approx \{2.12, 1.96, 1.93, 2.29, 1.83, 2.29, 1.87, 2.10\}$ (given in increasing order of $\Delta L_{\text{fold}} - \Delta L$); these are all consistent with the expected quadratic growth, $\beta = 2$. (b) Rescaling the data according to the power-law (S24) with $\beta = 2$, together with the best fit line over the first 5 points in each case (dotted lines). This allows the start time of snapping, t_0 , to be determined from the intercept with the horizontal axis.

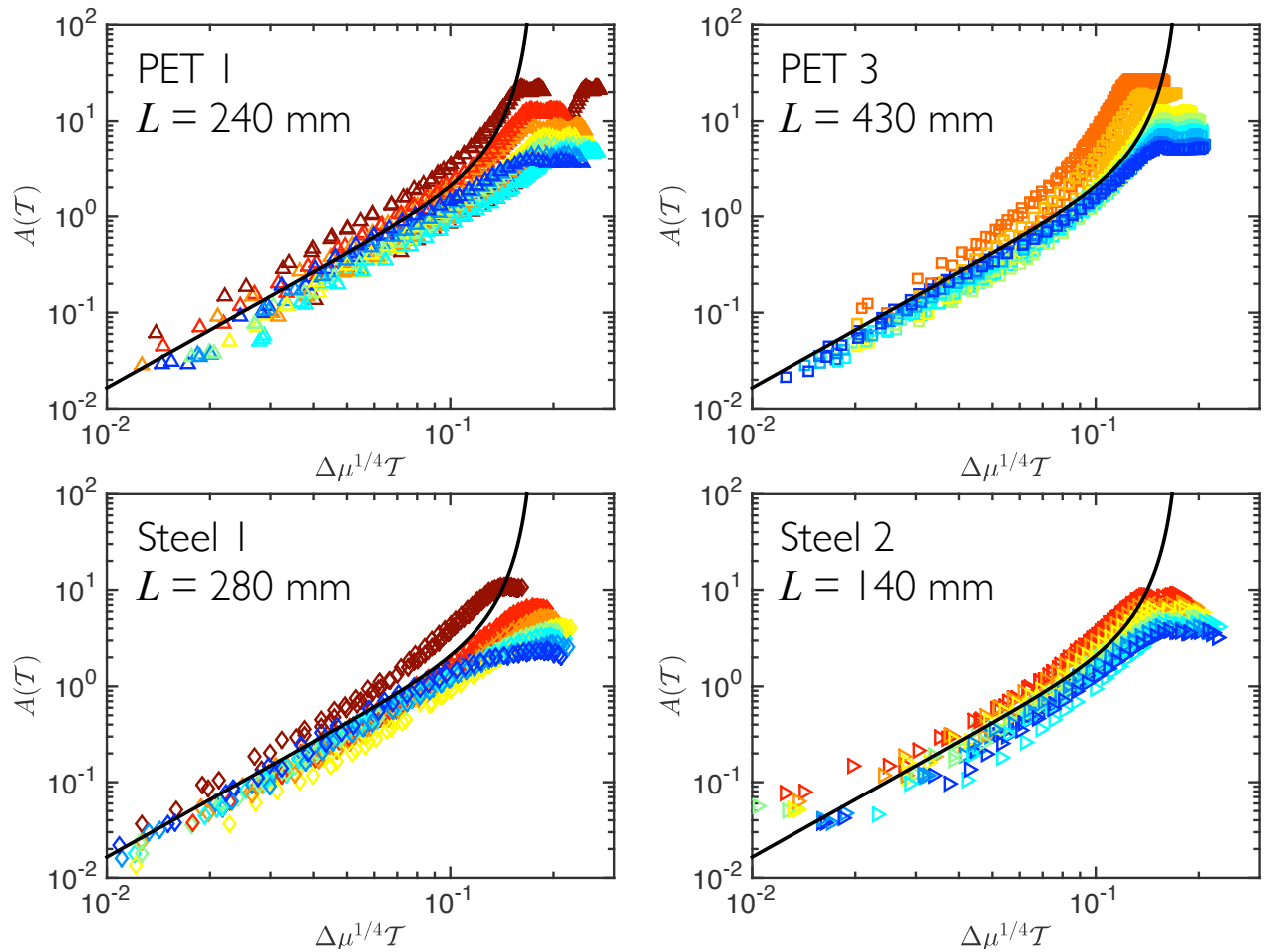


FIG. S5. Dimensionless midpoint trajectories during snapping for PET and steel strips of varying natural length L . In each plot, different trajectories correspond to different end-shortenings beyond the snapping transition, coloured as a heat-map from small values of $\Delta\mu$ (brown/red) up to large values of $\Delta\mu$ (blue). Data is shown for PET strips with $L = 240$ mm, $\alpha = 21.34^\circ$ (upward-pointing triangles) and $L = 430$ mm, $\alpha = 21.17^\circ$ (squares), as well as for experiments on steel strips with 280 mm, $\alpha = 17.14^\circ$ (diamonds) and $L = 140$ mm, $\alpha = 22.51^\circ$ (right-pointing triangles).